Modified Range Doppler Algorithm for CTSSAR

Yi Liao, Guoan Bi

***Abstract*—**Circular Scanning Trace Synthetic Aperture Radar (CTSSAR) employs circular flight path to constantly receive echo signals from the illuminated scene for obtaining a larger imaging area than that achieved by the conventional stripmap SAR. For this benefit of fast large-area imaging, however, the CTSSAR has a complex range history that introduces difficulties in target focusing. In order to address this problem, this paper investigate the range equation and propose a modified range Doppler algorithm tailored for CTSSAR based on higher range order approximation. The simulation results validate the effectiveness of the proposed approach.

Keywords-CTSSAR; ragne history; spectrum; modified range Doppler algorithm;

I. INTRODUCTION

With the development of microwave imaging technique, the synthetic aperture radar (SAR) has been widely used in both civil and military applications [1]-[3]. Conventional stripmap SAR travels along a straight flight path parallel to the ground at a constant flight speed. The antenna beam configuration employs side-looking mode [4]-[6]. For some particular applications, a bigger sensing area is needed during a short period, such as battlefield surveillance and mine detection. Circular trace scanning SAR (CTSSAR) has a circular flying trajectory with its beam footprint forming an annular illuminated area [7]. The circular area is generally larger than the one scanned by stripmap SAR within the same observation period, i.e., fast imaging a bigger area.

This benefit of fast imaging by the curved trajectory of CTTSAR is achieved at the cost of other difficulties in the imaging process. In the stripmap SAR processing, the Fresnel approximation is adopted for the expansion of range history, while is not possible for the CTSSAR [4]. The curved flight trajectory of CTSSAR brings higher order terms of phase error into the range equation so that the Fresnel approximation is not accurate enough to present the variation of the range history. A more accurate range approximation method is needed for CTSSAR imaging. To address the complex range path approximation, a pixel-to-pixel time domain integration algorithm seems to be a plausible solution. A well-matched filter can deal with very complicated range configuration, while the computation load becomes a serious issue for practical engineering applications [8]. The point to point matching generally results in a huge amount of redundant computation.

The authors are with the School of Electrical and Electronic Engineering, Nanyang Technological University, Singapore, 639798, liaoyi@ntu.edu.sg, egbi@ntu.edu.sg

To avoid the high computation load, the fast back projection method gives another choice for CTSSAR imaging. The approach utilizes subaperture imaging and image fusion to prevent the scene reconstruction from redundant phase computation operation [9]. Although the computation efficiency has been improved, the required computational time still appears too long compared with the frequency domain based algorithms. A high-speed chirp scaling algorithm is provided in [10] to investigate into CTSSAR target focusing. The wave front construction algorithm is also given to implement the CTSSAR imaging [11]. Both algorithms resort to the frequency information of the echo signal and obtain better computational efficiency. However, the range models of both approaches are based on quadratic approximation, which is not suitable in the high-resolution imaging.

In this paper, a higher order range approximation model is presented to accurately fit the real range history. The two-dimensional spectrum of CTSSAR is expanded via the stationary phase method. A modified range Doppler algorithm is then designed for the CTSSAR imaging process. Since the modified range Doppler algorithm is based on frequency domain processing, the range curvature can be removed simultaneously, alleviating the huge computational cost needed in temporal algorithm processing.

This paper is organized as follows. Section Ⅱ briefly reviews the signal model of the CTSSAR imaging mode. Section III discusses about the two-dimensional spectrum of the CTSSAR. Section IV presents a modified range Doppler imaging algorithm. Section V gives simulation results of the proposed approach, which validates the effectiveness of the proposed algorithm. Section VI presents the conclusions of this paper.

II. SIGNAL MODEL

A. Geometry of CTSSAR

The geometry of CTSSAR is provided in a 3D view in Fig. 1. The radar on platform A flies along a circular path at a certain height with a fixed side-looking beam outwards the circle. It is easy to find that, with the same flight duration, the circular observation area is larger than that of the straight-line flight. Herein, θ is the aspect angle, t_m is the slow time, and ω is the angular speed. Let us assume that P is an arbitrary target point with coordinates denoted by ($r_p\cos\theta_p$, $r_p\sin\theta_p$, 0). The position of A is ($r_a\cos\theta$, $r_a\sin\theta$, H), B and C denote the nearest and farthest range of the observation area, respectively.

Assuming that the slow time is zero when θ is equal to θ_p, we have $\theta = \theta_p + \omega t_m$. According to the geometric relationship, it is obvious that

$$R(\mathrm{t}_m) = \sqrt{H^2 + r_p^2 + r_a^2 + 2r_a r_p \cos(\theta - \theta_p)} \tag{1}$$

or

$$R(\mathrm{t}_m) = \sqrt{H^2 + r_p^2 + r_a^2 + 2r_a r_p \cos \omega \mathrm{t}_m} \tag{2}$$

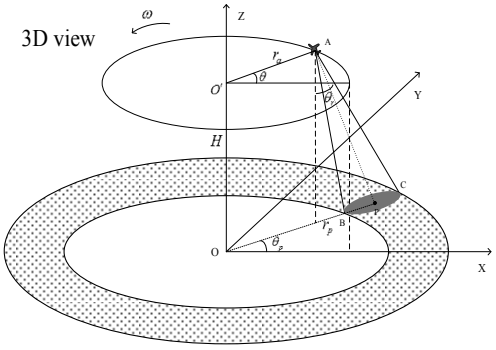

Figure 1. Geometry of CTSSAR

In order to analyze the range equation more clearly, Taylor expansion is applied to the instantaneous range. Let $R_0 = \sqrt{H^2 + (\mathrm{r}_p - \mathrm{r}_a)^2}$, we have

$$R(\mathrm{t}_m) = \mathrm{R}_0 + c_1 t_m + c_2 t_m^2 + c_3 t_m^3 + c_4 t_m^4 + \ldots \tag{3}$$

where c_1 , c_2 , c_3 and c_4 are coefficients of the different order terms of the Taylor series, expressed as

$$\begin{cases} c_1 = 0 \\ c_2 = \dfrac{r_a r_p \omega^2}{2R_0} \\ c_3 = 0 \\ c_4 = -\dfrac{\omega^4 r_a r_p}{24R_0} - \dfrac{\omega^4 r_a^2 r_p^2}{8R_0^3} \end{cases} \tag{4}$$

B. Echo signal

Let the transmitted radar signal be linear frequency modulated (LFM) signal, the chirp rate be γ , and the pulse width be T_p. Then the received echo signal from the ground target point P can be expressed as

$$s(\mathrm{t}, \mathrm{t}_m) = \sigma a_r \left[\mathrm{t} - \frac{2R(\mathrm{t}_m)}{c} \right] \mathrm{a}_a(\mathrm{t}_m) \exp\left\{ \mathrm{j}\pi\gamma \left[\mathrm{t} - \frac{2R(\mathrm{t}_m)}{c} \right]^2 \right\} \exp\left[-j \frac{4\pi}{\lambda} R(\mathrm{t}_m) \right] \tag{5}$$

where σ is the complex reflectivity, a_r and a_a are the range and azimuth of the waveform, respectively, λ is the wavelength of the carrier frequency and c is the light speed.

By performing the fast Fourier transform to the received signal, the echo signal is then converted into range frequency domain,

$$s(\mathrm{f}_r, \mathrm{t}_m) = \sigma \mathrm{A}_r(\mathrm{f}_r) \mathrm{a}_a(\mathrm{t}_m) \exp\left[-j \frac{4\pi(\mathrm{f}_c + \mathrm{f}_r) \mathrm{R}(\mathrm{t}_m)}{c} \right] \exp(-\mathrm{j} \frac{\pi f_r^2}{\gamma}) \tag{6}$$

where f_r is the fast frequency corresponding to fast time, f_c is the carrier frequency, and $A(\mathrm{f}_r)$ shows the Fourier transform of range waveform a_r . The two-dimensional spectrum, $s(\mathrm{f}_r, \mathrm{f}_a)$, of the echo signal can then be achieved through the stationary phase method as

$$s(\mathrm{f}_r, \mathrm{f}_a) = \int_{-\infty}^{+\infty} s(\mathrm{f}_r, \mathrm{t}_m) \exp(-\mathrm{j}2\pi \mathrm{f}_a \mathrm{t}_m) \mathrm{dt}_m \tag{7}$$

And the phase of (7) is

$$\theta(\mathrm{t}_m) = -\frac{4\pi(\mathrm{f}_c + \mathrm{f}_r) \mathrm{R}(\mathrm{t}_m)}{c} - \frac{\pi f_r^2}{\gamma} - 2\pi f_a t_m \tag{8}$$

Based on the stationary phase principle, the derivative of $\theta(t_m)$ can be obtained with respect to t_m . By setting it to zero, we have

$$f_a = \frac{2(\mathrm{f}_c + \mathrm{f}_r)\omega \mathrm{r}_a r_p \sin \omega t_m}{c\sqrt{r_a^2 + H^2 + r_p^2 - 2r_a r_p \cos \omega t_m}} \tag{9}$$

It is difficult to get the stationary phase t_0 based on (9) due to the fact that the flight curvature results in the high order range term in the spectrum phase error.

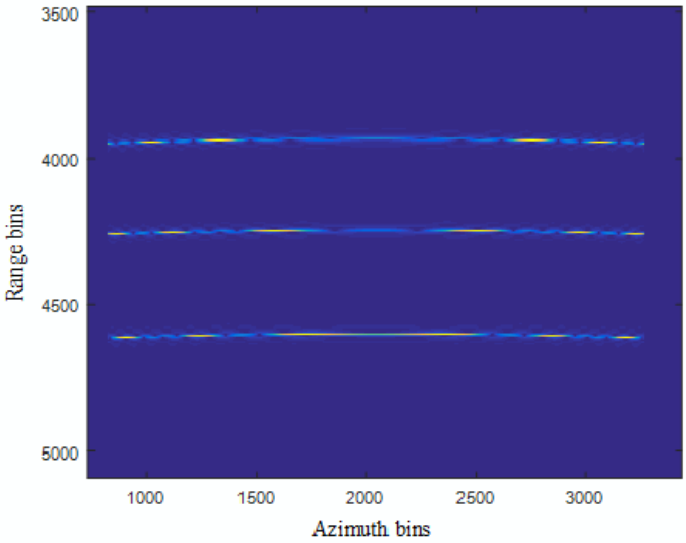

Fig. 2. Range curvature before correction

III. TWO-DIMENSIONAL SPECTRUM

To access to the 2-D spectrum, several approaches can be employed. Based on the stationary phase property, the solution can be obtained via solving the high order mathematic equation. By using the method of series reversion, the stationary phase point has a polynomial expression, further facilitating the analysis of the spectrum [12]. In addition, the implicit function method is also a good option for deducing the2-D spectrum [13].

Considering different order terms take different roles in the spectrum, the 2-D spectrum of the signal is expanded as a Taylor series.

$$\psi(f_r, f_a) = -\frac{4\pi(f_c + f_r)R_0}{c} + \phi_0(f_a) + \phi_1(f_a) f_r + \phi_2(f_a) f_r^2 + \phi_r(f_r) + \phi_{res} \quad (10)$$

The first term in (10) presents the linear phase indicating the point target's position and the constant term. ϕ_0 is the azimuth modulation term, the azimuth compression should be operated in range Doppler domain due to the coupling between range and azimuth. ϕ_1 is the range migration term and ϕ_2 is the secondary range compression term. Both terms result in the target focusing in image domain, and it is necessary to remove these two terms. ϕ_r is the range modulation term, it is easy to construction a matched filter in the 2-D frequency domain to implement range compression. Fig.2 shows the curved range history after range compression.

From Fig. 2, it is seen that the signal has been compressed into three curves for simulating three point targets. Since the existence of the range migration, the range history is not a straight line. The last term ϕ_{res} is the residual high order phase error term due to the impact of the circular flight in CTSSAR. In this paper, different from the conventional SAR imaging algorithm, the residual phase error term in the 2-D spectrum has been taken into consideration. A corresponding compensation function is designed for the residual high order term phase compensation. Fig. 3 presents the range history after the removal of the high order residual phase errors. It is noted that, in Fig. 3, the range cell migration and the secondary range compression have all been compensated. In comparison, Fig. 4 provides the range curve without the residual phase error compensation, which is, the idea of the traditional range Doppler method. It can be seen from the figure that the target is not well focused along range direction because the impact of the high order phase error term.

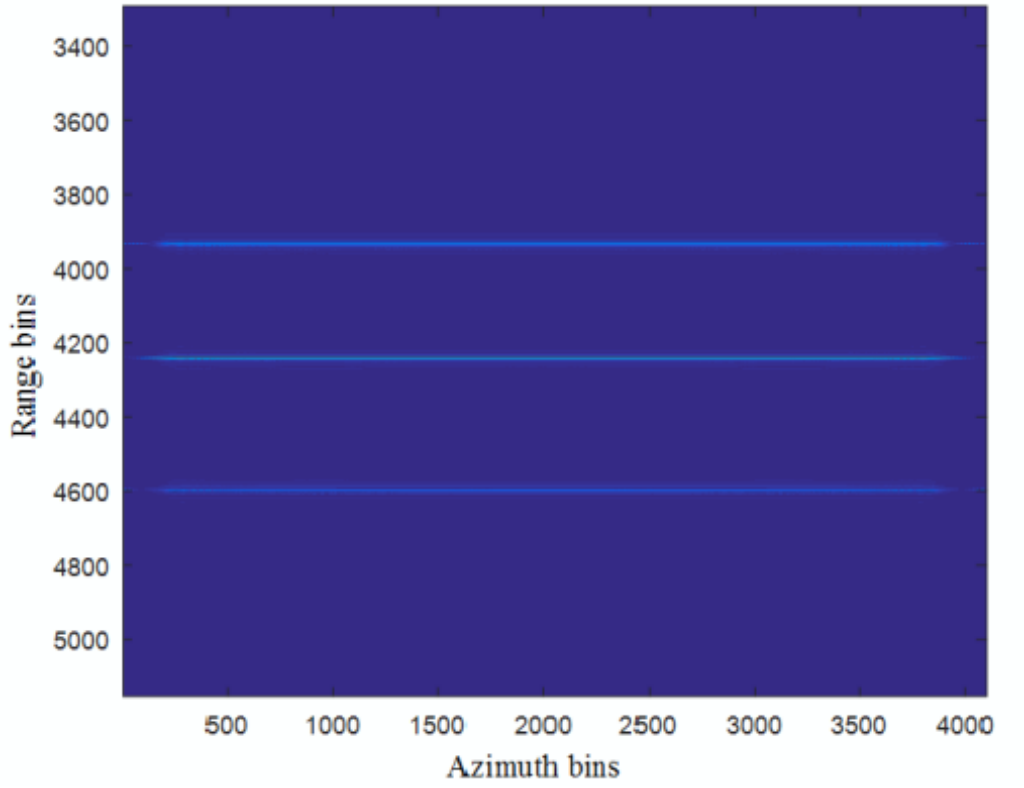

Fig. 3. Range history after migration correction

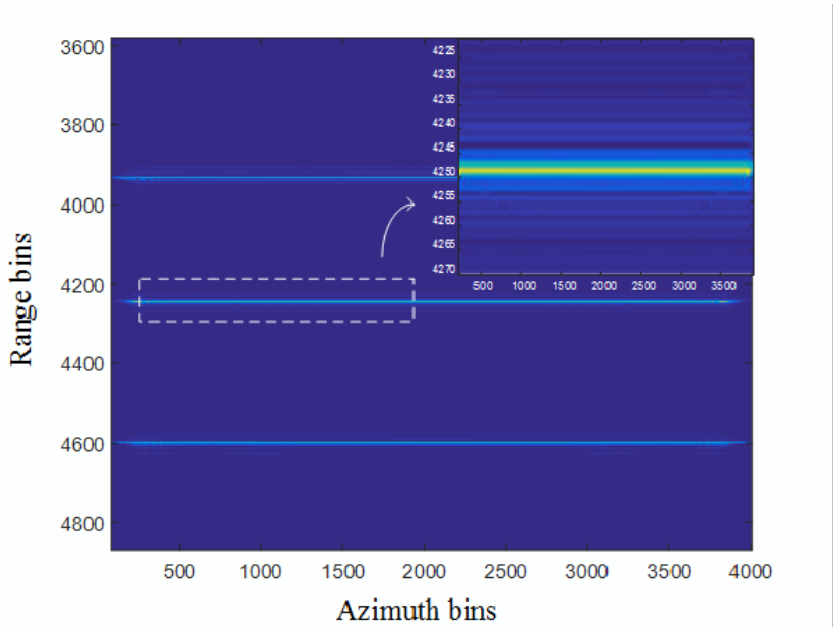

Fig. 4. range history without residual phase correction

IV. IMAGING ALGORITHM

Based on the derived 2-D spectrum shown in (10), the corresponding imaging algorithm is then developed. Considering the special character of CTSSAR and the principle of range Doppler algorithm, the range compression can be performed first. Then the echo signal is transformed into the 2-D frequency domain. The high order residual phase error from the circular trajectory could be removed by compensation function. Furthermore, the secondary range compression term can also be compensated in the 2-D frequency domain. The reference function is the conjugate of the secondary range compression term.

$$H_{src}(\mathrm{f}_a) = -\frac{\pi c f_a^2}{4c_2 f_c^3} + \frac{3\pi c_4 c^3 f_a^4}{32 c_2^4 f_c^5} \tag{11}$$

Next, the range inverse FFT (IFFT) is performed to convert the data into the range Doppler domain. This step is important in the modified range Doppler algorithm. SAR processing is in fact a 2-D filtering, and the signal energy is allocated range dependently [14]. Therefore, range cell migration correction (RCMC) in Doppler domain is necessary for the accurate imaging. Since the RCMC is dependent on the relative azimuth position rather than actual azimuth position, it cannot be applied in the 2-D time domain. Fortunately, the RCMC is dependent on the absolute Doppler effect. It is easy to apply RCMC in the range Doppler domain. The truncated sinc interpolation can be employed to implement the time shift operation. The range history is adjusted to a straight line in the range space domain, which makes it possible for the next azimuth compression.

Now the targets are interpolated successfully so that each target occupies a single range unit in the range Doppler domain. Since the azimuth response is space-variant, the azimuth filter can be constructed in range Doppler domain to realize bulk azimuth compression. The azimuth matched filter can be presented as

$$H_{az}(\mathrm{f}_a) = -\frac{\pi c f_a^2}{4c_2 f_c} + \frac{\pi c_4 c^3 f_a^4}{64 c_2^4 f_c^3} \tag{12}$$

Fig. 5 shows the imaging result after azimuth compression. It is obvious that all the azimuth cells are well focused. The last step of the algorithm is azimuth IFFT to transform the data into azimuth-space domain, i.e. the final image is formed in the time-space domain.

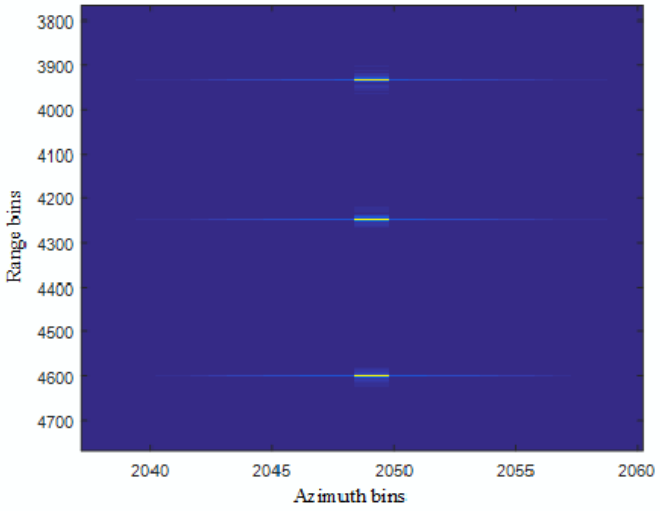

Fig. 5. Focused target after azimuth compression

Fig. 6 presents the flow chart of our proposed algorithm.

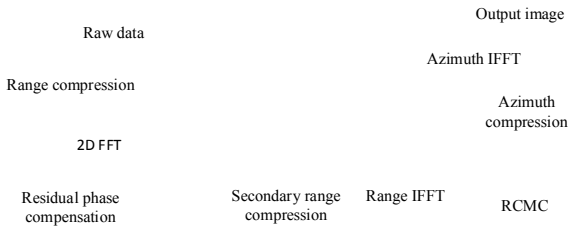

Fig. 6. Flow chart of the proposed algorithm

V. SIMULATIONS

Simulations are carried out to validate the effectiveness of the proposed algorithm. In the simulation, three point targets are placed in the imaging scene. One is located in the center of the scene and the other two points are 500m away from the reference point. The X band radar has a wavelength of 0.03m, a signal bandwidth of 300MHz, a sampling rate of 500MHz and a pulse width of 10 μs . The azimuthal beamwidth is 5°, the flight height is 2000m, flight speed is 100m/s, and the pulse repetition frequency (PRF) is 1kHz. The three point imaging results can be found in Fig. 5. The focusing contour for one point target is given in Fig.7. The figure clearly shows that the target is focused perfectly because the proposed modified range Doppler algorithm takes the range variance. Due to the circular trajectory happened in CTSSAR, into consideration. The residual high order term of the phase error is accurately removed from the 2-D spectrum domain. The RCMC is implemented in the range Doppler domain, correcting the space variant migration to a same unit. The final image is achieved in time-space domain.

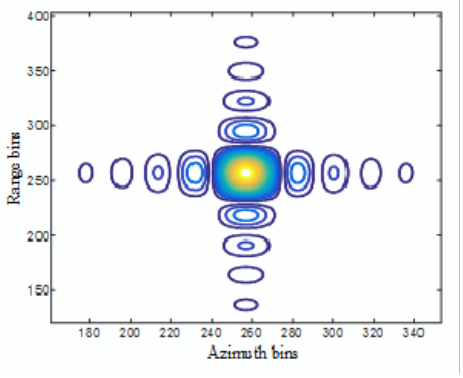

Fig. 7. Imaging result with the proposed algorithm.

In order to evaluate the imaging quality, the azimuth and range pulse responses are also provided. It is seen from Fig.8 that the peak sidelobe ratio for both azimuth and range are around -13dB, which is almost the same as the theoretical value. It further proves that the proposed imaging algorithm is feasible in the CTSSAR imaging process.

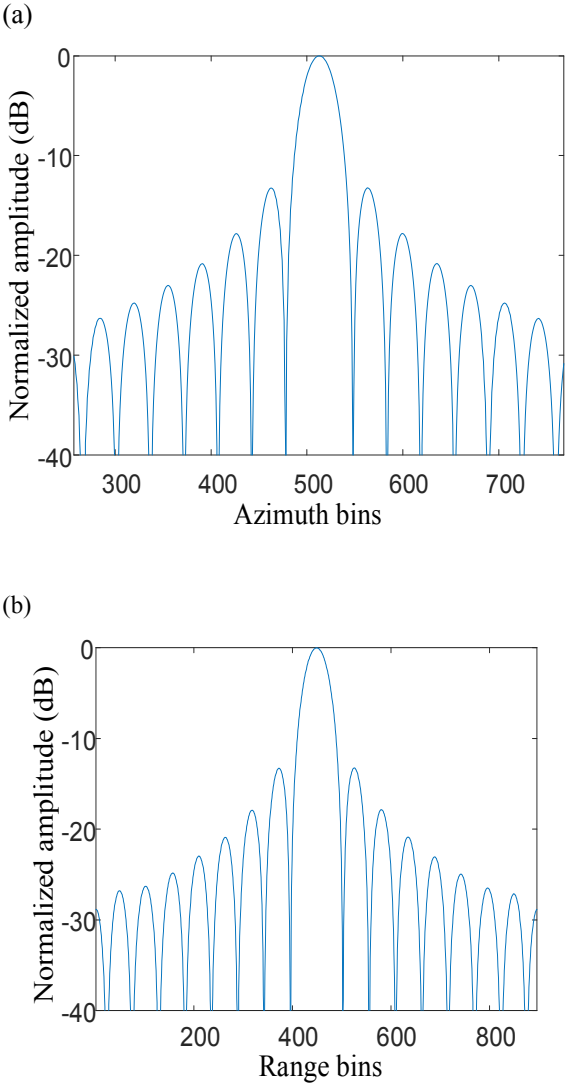

Figure 8. target pulse responses. (a) Azimuth. (b) Range.

VI. CONCLUSIONS

In this paper, a modified range Doppler algorithm suitable for the CTSSAR imaging is proposed. The impact of range variance in CTSSAR is well considered. The effects of high order terms are compensated in the 2-D frequency domain and the range cell migration is accurately corrected in the range Doppler domain. The entire algorithm can be easily applied for practical applications. The simulation imaging result demonstrates the feasibility and good performance of the proposed algorithm.

REFERENCES

[1] S. Zhou, L. Yang, L. Zhao and G. Bi, "Forward Velocity Extraction From UAV Raw SAR Data Based on Adaptive Notch Filtering," in *IEEE Geoscience and Remote Sensing Letters*, vol. 13, no. 9, pp. 1211-1215, 2016.

[2] L. Yang, G. Bi, M. Xing and L. Zhang, "Airborne SAR Moving Target Signatures and Imagery Based on LVD," in *IEEE Transactions on Geoscience and Remote Sensing*, vol. 53, no. 11, pp. 5958-5971, Nov. 2015.

[3] S. Zhou, M. Xing, X. G. Xia, Y. Li, L. Zhang and Z. Bao, "An Azimuth-Dependent Phase Gradient Autofocus (APGA) Algorithm for Airborne/Stationary BiSAR Imagery," in *IEEE Geoscience and Remote Sensing Letters*, vol. 10, no. 6, pp. 1290-1294, Nov. 2013.

[4] I. G. Cumming and F. H. Wong, Digital Processing of Synthetic Aperture Radar Data: Algorithms and Implementation (Artech House Remote Sensing Library). Norwood, MA, USA: Artech House, 2005.

[5] R. J. Curlander, "Synthetic aperture radar: Systems and signal processing," 1991.

[6] M. Soumekh, "Synthetic aperture radar," Signal Processing with MATLAB Algorithms. New York: John Wiley & Sons, Inc, 1999.

[7] Y. Liao, M. Xing, Z. Bao and Qing Huo Liu, "Analysis on parameters and imaging algorithm of squint circular trace scanning SAR," *2015 IEEE Radar Conference (RadarCon)*, Arlington, VA, 2015, pp. 0151-0155.

[8] A. Broquetas, R. Porrata, L. Sagues, X. Fabregas, and L. Jofre, 'Circular synthetic aperture radar (C-SAR) system for ground-based applications', *Electron. Lett.,* vol. 33, no. 11, pp. 988–989, 1997.

[9] L. M. H. Ulander, H. Hellsten, and G. Stenstrom, "Synthetic-aperture radar processing using fast factorized back-projection," IEEE Trans. Aerosp. Electron. Syst., vol. 39, no. 3, pp. 760–776, Jul. 2003.

[10] M. Bara, L. Sagues, Paniagua, A. Broquetas, and X. Fabregas, 'High-speed focusing algorithm for circular synthetic aperture radar', *Electron. Lett.,* vol. 36, no. 9, pp. 828–830, 2000.

[11] D., Garmatyuk, R. Narayanan, 'Ultra-wideband continuous-wave random noise Arc-SAR', *IEEE Trans. Geosci. Remote Sens*., 40, (12), pp. 2543-2552, 2002

[12] Y Liao, M Xing, L Zhang, and Z Bao. "A novel modified Omega-K algorithm for circular trajectory scanning SAR imaging using series reversion." *EURASIP Journal on Advances in Signal Processing*, 2013, no. 1 pp. 64.

[13] Y. Liao, W. Q. Wang and Q. H. Liu, "Two-Dimensional Spectrum for Circular Trace Scanning SAR Based on an Implicit Function," in *IEEE Geoscience and Remote Sensing Letters*, vol. 13, no. 7, pp. 887-891, July 2016.

[14] L. Yang, L. Zhao, G. Bi and L. Zhang, "SAR Ground Moving Target Imaging Algorithm Based on Parametric and Dynamic Sparse Bayesian Learning," in *IEEE Transactions on Geoscience and Remote Sensing*, vol. 54, no. 4, pp. 2254-2267, April 2016.